LATTICE BOLTZMANN SIMULATION OF THE PRANDTL NUMBER EFFECT ON THE PHASE CHANGE HEAT TRANSFER OF WAX IN PIPE-LINE

by

Xiaoyan LIU[a], Lingxiang KONG[a], Zheng ZHOU[b], Huanyu ZHANG[b], Xinghui SHE[a], Yongying JIA[a], Ying XU[a], and Hui JIANG[b*]

[a] School of Mechanical Science and Engineering,
Northeast Petroleum University, Daqing, China
[b] School of Civil Engineering and Architecture,
Northeast Petroleum University, Daqing, China

Original scientific paper
https://doi.org/10.2298/TSCI230706259L

Thermal washing is a common method of wax removal in oil fields. The law of phase change heat transfer of wax during the thermal washing process is revealed to be of great significance for improving the melting rate of wax. The lattice Boltzmann method is used to numerically simulate the process of phase change heat transfer in pipe-lines with different angles (90°, 45°, 0°, –45°, and –90°) of wax layers based on the enthalpy-porous medium model in the present work. The boundary condition between wax and hot water is considered as convective heat transfer boundary. The effect of the Prandtl number on the law of phase change heat transfer of the wax at various angles is investigated. The simulation results indicate a non-linear decrease in the complete melting time of the wax layer from –90° to 90°. The heat transfer capacity is enhanced with the decrease of Prandtl number, which effectively shortens the melting time of wax. The complete melting time of the wax layer is reduced by 23.78% when the Prandtl number decreases from 79.4-59.4. The speed of convective heat transfer is increased with the decrease of Prandtl number, which means that the solid zone of wax is accelerated into the loose and porous mushy zone, and the efficiency of wax removal is improved. The research results can provide a reference for improving the efficiency of thermal washing.

Key words: *lattice Boltzmann method, phase change, angle, Prandtl number*

Introduction

Wax deposition is a prevalent issue during oil production and transmission, and solving the problem of wax deposition in waxy crude-oil pipe-lines has received extensive attention [1, 2]. Currently, most of the world's crude-oil is crude-oil containing large amounts of wax [3, 4]. During the transportation of crude-oil, when the temperature of the pipe-line wall drops below the wax appearance temperature, dissolved wax in proximity toes supersaturation, leading to crystallization and precipitation. These precipitates gradually diffuse towards the inner wall of the pipe-line, eventually forming a deposition layer composed of waxes [5]. Waxing not only leads to problems such as increased transportation costs and pipe-line clogging [6], but also seriously affects oilfield safety and efficient production. Therefore, effective wax removal is of great importance to ensure safe production and reduce crude-oil production costs.

* Corresponding author, e-mail: 18345969135@163.com

There are mainly thermal washing, mechanical, chemical, microbiological and electromagnetic methods for wax removal [7-11]. The thermal washing method is widely used in the oil field because of its simple operation and low cost. Research on thermal washing wax removal has both experimental and simulation aspects. The velocity and temperature of the thermal washing medium were studied for the effect of wax removal in the thermal washing wax removal experiment. However, microscopic information on the internal heat transfer and flow during the phase change of wax is difficult to be obtained through experimental studies, and there are more interference factors in the experimental process. Numerical simulation is regarded as a valuable supplement to the experimental study, which can obtain detailed information about the phase transition process of wax at different positions of the pipe-line and help to analyze the law of wax melting.

In the context of numerical simulation, the effects of water temperature, flow velocity, wax layer thickness, and natural-convection on the melting of wax layers in pipe-lines have been investigated using traditional CFD methods [7, 12]. Li *et al*. [13] also studied the melting and flow characteristics of spherical wax blocks in pipe-lines. The effect of the Prandtl number, and Rayleigh number, on the melting of wax in tubes has been studied using the lattice Boltzmann method in recent years [2, 14]. However, the influence of relevant factors on the overall melting of the wax layer in the axial or diameter direction was analyzed in the aforementioned study. The phase change heat transfer law of locally located wax layers has not been investigated. It is necessary to study the different positions of the wax layer circumferentially and then reveal its melting mechanism due to the circumferential non-uniformity of the wax layer during the melting process.

In comparison the CFD method, the lattice Boltzmann method emerges as a highly effective mesoscopic numerical simulation technique due to its exceptional capability in handling intricate geometries and boundary conditions, along with its inherent parallelism [15]. It is widely used in the fields of porous media flow, heat transfer and solid-liquid phase change [16-18]. Relevant studies in the field of energy storage can be referenced by the study of pipeline thermal wash wax removal, because the solid-liquid phase change process of PCM has characteristics similar to the melting of wax in pipe-lines. The solid-liquid phase change process of PCM in rectangular [19], spherical [20], and annular [21] cavities with different shapes has been extensively studied in the field of energy storage. Some scholars have investigated the effects of different heating positions [22, 23], and cavity tilt angles [24, 25].

The wax in the oil pipe-line belongs to the mixture. The interval between the liquid and solid zones of the wax is called the mushy zone. The convection caused by the flow of the liquid and mushy zones makes the coupling between flow and heat transfer more complicated. For this complex phase change coupling solution, Voller *et al.* [26] proposed a solution method for the mushy zone in the phase change problem based on the enthalpy method and the fixed grid method, and regarded the mushy zone as a porous medium following Darcy's law, and proposed the enthalpy-porous medium model for the first time. Su and Davidson [27] proposed a dimensionless lattice Boltzmann method with adjustable mesoscopic time steps applicable to phase change flow and heat transfer. The interface between fluid and solid is regarded as a mushy zone with transient porosity change. The seepage study of porous media mainly focuses on the pore and representative elementary volume (REV) scales. The information of the phase change and heat transfer flow process is obtained based on the pore scale will need to be studied on the basis of obtaining the pore structure data of porous media, which has the problem of sizeable computational volume and inability to achieve large-scale computation. The lattice Boltzmann model at the REV scale can be constructed by introducing physical parameters

such as porosity, specific heat capacity, and force terms that reflect the influence of porous media into the model without requiring detailed structural information of the substance. The specific structure inside the wax cannot be obtained, so it is more effective to study the mushy zone of wax based on the REV scale. Guo and Zhao [28] proposed a lattice Boltzmann model corresponding to the generalized seepage model at the REV scale. Seta *et al*. [29] verified the reliability and computational efficiency of lattice Boltzmann in simulating natural-convection in porous media at the REV scale. Gao and Chen [30] developed a lattice Boltzmann model capable of simulating the natural-convection melting problem in porous media at the REV scale. They simulated the melting process of pure matter in a rectangular cavity with and without a filled porous medium, and the simulation results agreed well with the analytical solution better. Therefore, the mushy zone of the wax phase change process is simplified as a porous medium for treatment is feasible based on the REV scale.

In summary, the majority of studies have focused on the melting of the wax layer axially or radially overall. However, the circumferential direction of wax melting in the pipe-line shows a non-uniform distribution. The law and mechanism of the influence of Prandtl number on the melting process of wax at different angles are still unclear and need to be further investigated. Hence, the model of solid-liquid phase change heat transfer and flow processes in the circumferential local position of the wax layer and the double distribution lattice Boltzmann model based on the enthalpy-porous medium model are established in this paper. The effect of Prandtl number on the phase change heat transfer law of wax at different angles of the wax layer is investigated.

Mathematical modelling

Physical model

The problem of phase change heat transfer in the wax layer in the pipe-line is simplified to a 2-D radial heat transfer, while neglecting the axial heat transfer along the pipe-line. Five representative wax layer angles at 90°, 45°, 0°, –45°, and –90° are chosen for the right half of the pipe due to the symmetry of the pipe-line and the non-uniformity of the circumferential melting. The radial cross-section of the crude-oil pipe-line is depicted in fig. 1(a). Figure 1(b) shows the local physical model of the melting of the wax layer in the pipe-line. The melting process of wax was partitioned into liquid, mushy and solid zones. The initial temperature of the wax layer is T_p = 298.15 K, and the hot water temperature is constant at T_f = 368.15 K. The interface between hot water and wax is defined as the heat exchange surface. The hot water and wax do not mix during the melting process, and the convective heat transfer boundary is set between the hot water and wax. The outer wall of the pipe-line is simplified as an adiabatic boundary.

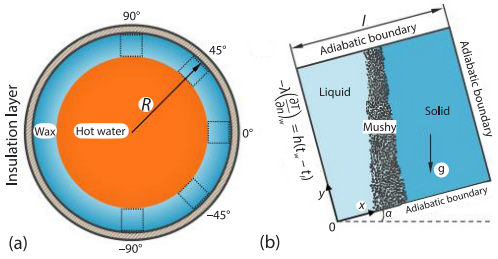

Figure 1. Physical model; (a) pipe-line cross-section diagram and (b) local physical model of wax layer melting

Governing equations

The mathematical model is based on the following assumptions: Ignoring the viscous heat dissipation during the flow of liquid wax. The thermal properties of wax in the solid and liquid phases are considered to be constant. The liquid wax is regarded as an incompressible

Newtonian fluid. The density variation in the body force term follows the Boussinesq assumption. The fluid density, ρ:

$$\rho = \rho_0 \left[1 - \beta_T (T - T_{\text{ref}})\right] \tag{1}$$

where ρ_0 and T_{ref} are the average fluid density and reference temperature, respectively and β_T is the coefficient of thermal expansion.

Continuity equation:

$$\nabla \mathbf{u} = 0 \tag{2}$$

Momentum equation:

$$\frac{\partial \mathbf{u}}{\partial t} + (\mathbf{u}\nabla)\frac{\mathbf{u}}{\varepsilon} = -\frac{1}{\rho_{\text{fl}}}\nabla(\varepsilon p) + \nu_e \nabla^2 \mathbf{u} + \mathbf{F} \tag{3}$$

Energy equation:

$$\left[\varepsilon\left(\rho c_p\right)_{\text{fl}} + (1-\varepsilon)\left(\rho c_p\right)_{\text{fs}}\right]\frac{\partial T}{\partial t} + \left(\rho c_p\right)_{\text{fl}}\left(\mathbf{u}\nabla T_f\right) = k_e \nabla^2 T - \varepsilon \rho_{\text{fl}} La \frac{\partial \gamma}{\partial t} \tag{4}$$

where ε and γ are porosity and liquid fraction, respectively. Porosity is obtained by the liquid fraction, $\varepsilon = \gamma$, ρ_{fl} – the liquid density of wax, p – the pressure, and ν_e – the effective kinematic viscosity. The subscripts fl and fs represent the liquid and solid phases of the PCM, respectively, k_e and La are, respectively, the effective thermal conductivity and the latent heat of fusion. The **F** is the total body force term containing linear and non-linear resistance and buoyancy force:

$$\mathbf{F} = -\frac{\varepsilon \nu_{\text{fl}}}{K}\mathbf{u} - \frac{\varepsilon F_\varepsilon}{\sqrt{K}}\mathbf{u}\,|\,\mathbf{u}\,| + \varepsilon \text{g}\beta_T\left(T - T_{\text{ref}}\right) \tag{5}$$

where ν_{fl}, K, and F_ε are the fluid dynamic viscosity, the porous medium permeability, and the shape factor, respectively.

Based on the enthalpy-porous medium model, the enthalpy and liquid fraction at each node of the wax layer were calculated:

$$En = c_p T + \gamma La, \;\; \gamma = \frac{En - En_s}{En_l - En_s} \tag{6}$$

where En, En_s, and En_l are the enthalpy of each node, the enthalpy corresponding to the initial melting temperature, T_{fs}, and the enthalpy corresponding to the melting completion temperature T_{fl}, respectively. In order to further explore the general law of phase change heat transfer of wax layer and reduce the influence of variables, the following dimensionless variables are introduced:

$$X = \frac{x}{L}, \quad Y = \frac{y}{L}, \quad \text{Fo} = \frac{\alpha t}{L^2}, \quad \text{Pr} = \frac{\nu_{\text{fl}}}{\alpha_{\text{fl}}}, \quad \text{Ra} = \frac{\text{g}\beta\left(T_h - T_c\right)H^3}{\nu_{\text{fl}}\alpha_{\text{fl}}}, \quad \text{Ste} = \frac{(c_p)_{\text{fl}}\left(T_h - T_c\right)}{L\alpha} \tag{7}$$

Lattice Boltzmann model

The convection term plays a crucial role in the fluid-flow problem. Since the D2Q4 or D2Q5 model cannot guarantee the macroscopic isotropy, the D2Q9 model of the double-distributed lattice Boltzmann method is adopted to solve the problem. The density distribution function is used to describe the velocity field, and the temperature distribution function is used to describe the temperature field. The velocity field is described using the generalized percolation model proposed by Guo and Zhao [31]. The evolution equation of the density distribution function is defined:

$$f_i\left(\mathbf{r} + \mathbf{e}_i \Delta t, t + \Delta t\right) - f_i(\mathbf{r}, t) = -\frac{1}{\tau_f}\left[f_i(r,t) - f_i^{\text{eq}}(r,t)\right] + \Delta t F_i \tag{8}$$

where $\mathbf{r}$ is the space vector position, t – time, $\mathbf{e}_i$ – the lattice discrete velocity, Δt – the time step, and τ_f – the dimensionless relaxation time in the velocity distribution function, $\tau_f = 3\nu_e/(c^2\Delta t) + 0.5$, f_i^{eq} and F_i are the equilibrium distribution function and the source term of the density distribution function, respectively, which are determined:

$$f_i^{\text{eq}} = w_i\rho\left[1+\frac{3\mathbf{e}_i\mathbf{u}}{c^2}+\frac{9(\mathbf{e}_i\mathbf{u})^2}{2\varepsilon c^4}-\frac{3\mathbf{u}^2}{2\varepsilon c^2}\right] \tag{9}$$

$$F_i = w_i\rho\left(1-\frac{1}{2\tau_f}\right)\left[\frac{\mathbf{e}_i\mathbf{F}}{c_s^2}+\frac{\mathbf{uF}:(\mathbf{e}_i\mathbf{e}_i-c_s^2\mathbf{I})}{\varepsilon c_s^4}\right] \tag{10}$$

where w_i is the weight coefficient, and in the D2Q9 model, $w_i = 4/9$ for $i = 0$, $w_i = 1/9$ for $i = 1$-4, and $w_i = 1/36$ for $i = 5$-8.

Fluid density and flow velocity are defined:

$$\rho = \sum_i f_i,\ \mathbf{u} = \sum_i \mathbf{e}_i f_i/\rho + \mathbf{F}\Delta t/2 \tag{11}$$

Since $\mathbf{F}$ contains flow velocity $\mathbf{u}$, eq. (11) is a quadratic non-linear equation of velocity, which can be solved:

$$\mathbf{u} = \frac{\mathbf{V}}{c_0+\sqrt{c_0^2+c_1|\mathbf{V}|}},\ \mathbf{V} = \sum_i \mathbf{e}_i f_i/\rho + \frac{\Delta t}{2}\varepsilon\left[\beta g(T-T_{\text{ref}})\right] \tag{12}$$

$$c_0 = \frac{1}{2}\left(1+\varepsilon\frac{\Delta t}{2}\frac{\nu}{K}\right),\ c_1 = \varepsilon\frac{\Delta t}{2}\frac{F_\varepsilon}{\sqrt{K}} \tag{13}$$

The temperature field adopts the lattice Boltzmann model of the non-linear convection diffusion equation proposed by Shi and Gao [32], and the temperature distribution function g_i is defined:

$$g_i(\mathbf{r}+\mathbf{e}_i\Delta t, t+\Delta t) - g_i(\mathbf{r},t) = -\frac{1}{\tau_T}[g_i(\mathbf{r},t) - g_i^{\text{eq}}(\mathbf{r},t)] + \Delta t S_i \tag{14}$$

where τ_T is the dimensionless relaxation time in the temperature distribution function, $\tau_f = 3\alpha_e/(c^2\Delta t\sigma) + 0.5$, g_i^{eq} and S_i are the equilibrium distribution function of temperature and the source term of the evolution equation of distribution function, respectively, which are determined:

$$g_i^{\text{eq}} = w_i T\left[1+3\frac{\mathbf{e}_i\mathbf{u}}{c^2\sigma}+4.5\frac{(\mathbf{e}_i\mathbf{u})^2}{c^4\sigma^2}-1.5\frac{\mathbf{u}^2}{c^2\sigma^2}\right] \tag{15}$$

$$S_i = -w_i\varepsilon\frac{La}{c_{p\text{fl}}\sigma}\frac{[\gamma(t+\Delta t)-\gamma(t)]}{\Delta t}\left[1+\left(1-\frac{1}{2\tau_T}\right)\frac{3\mathbf{e}_i\mathbf{u}}{\sigma c^2}\right] \tag{16}$$

The macroscopic temperature is calculated:

$$T = \sum_i g_i \tag{17}$$

Boundary conditions for lattice Boltzmann method

For the convective heat transfer boundary condition, t_w is obtained, and then the unknown distribution function at the boundary is calculated by the same treatment scheme as the Dirichlet boundary [33]:

$$g_i(r,t+\Delta t) = -g_i(r,t) + 2w_i t_w \tag{18}$$

For the adiabatic boundary, the temperature at the boundary is equal to the temperature of the adjacent layer [24]:

$$g_i(n,t) = g_i(n-1,t), \ \ i = 0,8 \tag{19}$$

For the velocity boundary, the boundary of the selected local model is assumed to be a no-slip boundary, and the bounce back scheme is used for processing.

Physical parameters of wax

The physical parameters of wax measured by experiment are shown in tab. 1. Numerical simulations were performed based on tab. 1.

Table 1. Physical parameters of wax

Parameters	Values
Density of liquid phase [kgm^{-3}]	768.32
Density of solid phase [kgm^{-3}]	905.71
Thermal conductivity of liquid phase [Wm^{-1}K^{-1}]	0.15
Thermal conductivity of solid phase [Wm^{-1}K^{-1}]	0.24
Specific heat capacity of liquid phase [kJkg^{-1}K^{-1}]	2.10
Specific heat capacity of solid phase [kJkg^{-1}K^{-1}]	1.75
Dynamic viscosity [Pa·s]	$4.96 \cdot 10^{-3}$
Phase change temperature region [K]	309.55-315.35
Latent heat [Jkg^{-1}]	$1.87 \cdot 10^{5}$

Validation

Grid independence verification

In order to ensure the independence of the number of grids used in the simulation, five different grid sizes (60 × 60, 80 × 80, 100 × 100, 120 × 120, 140 × 140) were selected for independent verification. The change of liquid fraction of wax in the square cavity was calculated for Ra = 1×10^6 and Ste = 0.84, and the results are obtained as shown in fig. 2. It can be seen that the difference in the variation of the liquid fraction decreases with increasing the grid sizes. The deviations of Fourier numbers for grids with dimensions of 60 × 60, 80 × 80, 100 × 100, and 120 × 120 relative to those with dimensions140 × 140 are observed to be 7.19%, 2.70%, 0.81%, and 0.34%, respectively. The errors of 100 × 100 and 120 × 120 grids exhibit a high degree of similarity to those of 140 × 140 grids, thereby satisfying the requirement for grid independence. The grid size of 100 × 100 is selected for numerical calculations for improving computational efficiency.

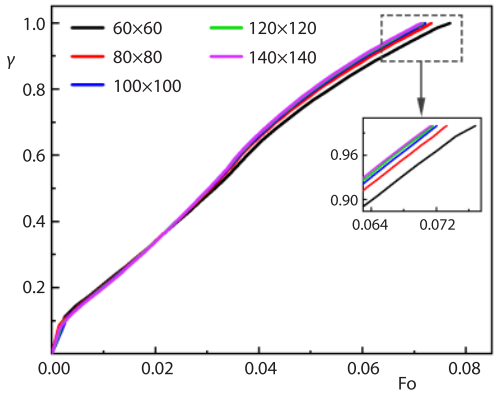

Figure 2. Grid independence verification

Visual experimental verification

To verify the accuracy of the model, a visualization experiment was taken to compare with the numerical simulation results. The dimensions of the square chamber device in the experiment are 30 mm × 30 mm × 30 mm, and the square chamber is filled with wax. The left side of the square cavity was heated at 338.15 K, and the rest of the surfaces were adiabatically treated with thermal insulation cotton. The initial temperature of the wax was 283.15 K. The changes of the melting phase interface and liquid fraction in the square cavity were recorded and compared with the numerical simulation results. The results of the visual experiments are shown in figs. 3(a) and 3(c), and the results of the numerical simulations are shown in figs. 3(b) and 3(d). The existence of the mushy zone can be clearly observed through experimental snapshots, and the experimental results are close to the simulation results. The absolute errors for Fo = 0.622 and Fo = 0.870 are 2.74%, and 1.54%, respectively.

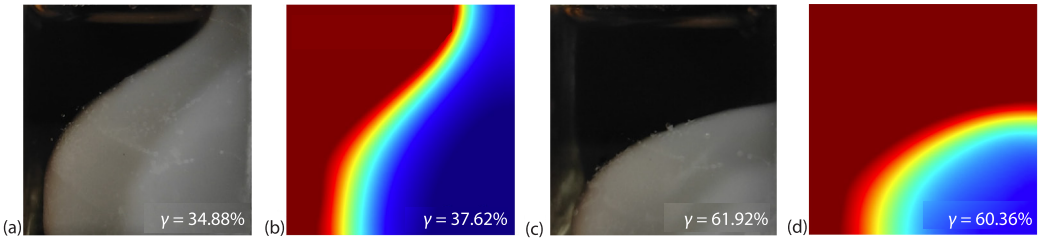

Figure 3. Results of visualization experiment and numerical calculation; (a) and (b) Fo = 0.622 and (c) and (d) Fo = 0.870

Table 2 shows the wax liquid fraction values of visualization experiments and numerical calculations at other different times. The maximum absolute error and average absolute error of the liquid fraction of wax in the visual experiment and numerical simulation are 2.74% and 1.48%, respectively. The model meets the accuracy requirements. The grid independence verification and visualization experiments show that the model has good accuracy.

Table 2. Comparison of errors in visualization experiments and numerical calculation of liquid fraction

Fourier number	Numerical calculation of liquid fraction [%]	Experimental liquid fraction [%]	Error [%]
0	0	0	0
0.184	11.84	12.59	0.75
0.432	24.01	21.66	–2.35
0.622	37.62	34.88	–2.74
0.870	60.36	61.90	1.54

Results and discussions

The Prandtl number represents the capacity for momentum diffusion and heat transfer. It reflects the influence of fluid physical properties on flow and heat transfer. Exploring the influence of Prandtl number on the heat transfer law of wax phase change in the pipe-line is helpful to analyze the mechanism of the relative speed of momentum and heat diffusion on the wax phase change process. The Prandtl number of wax is 69.4 from tab. 1. The Pr = 59.4 and

79.4 were selected for comparison with Pr = 69.4 to investigate the impact of the size of the Prandtl number on the heat transfer pattern of wax phase change in the pipe-line.

Effect of Prandtl number on local convective characteristics

The temperature field and velocity vector distribution at the moments of Fourier numbers of 0.006, 0.029, and 0.052 for the three Prandtl numbers are shown in fig. 4-6, respectively.

As shown in fig. 4, the temperature field patterns at all angles of the wax layer at the three Prandtl numbers are similar, and the isotherms are uniformly distributed and approximately parallel to the heat transfer surface at Fo = 0.006. Heat transfer in wax is dominated by thermal conductivity in the early stage of melting and the heating time is short, the effect of Prandtl number on the temperature field of the wax layer at all angles is not obvious. From the distribution of the velocity vector, it can be seen that the vortices in the velocity vector distribution at 45°, 0° and –45° positions of the wax layer under the three Prandtl numbers all show an oblong shape and are more regular. The velocity of the wax near the heat exchange surface is greater at 90°, while the flow rate of the wax is approximated as 0 at –90°. The flow of liquid wax gradually diminishes from 90° to –90° as the direction of the heat source transitions from aligning with the buoyancy force to opposing it, resulting in varying distributions of velocity vectors.

The direction of the heat source gradually shifted from the same direction as the direction of the buoyancy force to the opposite from 90° to –90° as shown in fig. 5. The convection effect shifts from maximum to being completely suppressed, and the melted liquid wax

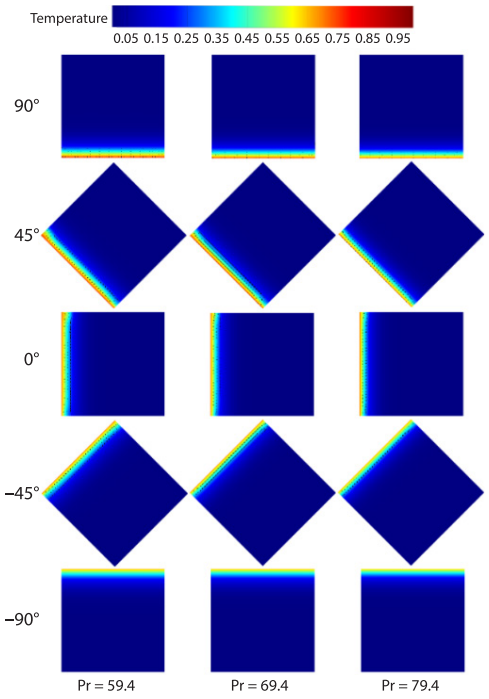

Figure 4. The temperature field (contour) and velocity vector distribution (arrow) of wax at different angles under different Prandtl numbers, (Fo = 0.006)

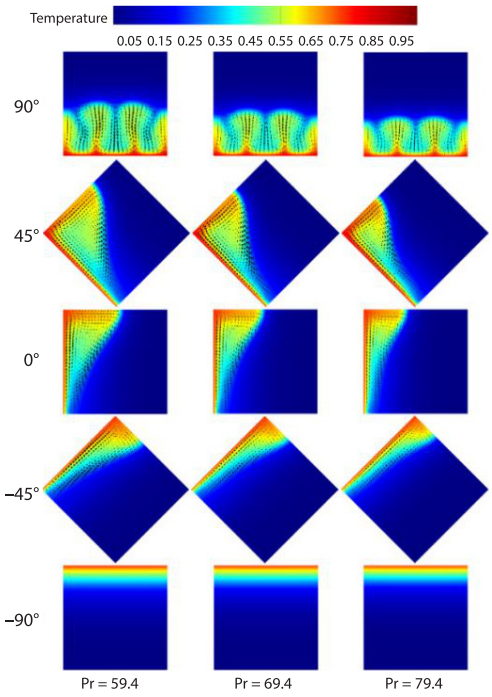

Figure 5. The temperature field (contour) and velocity vector distribution (arrow) of wax at different angles under different Prandtl numbers, (Fo = 0.029)

gradually decreases. The temperature field and velocity vector distribution can be clearly observed at the 90° position of the pipe-line. The temperature field has two more pronounced full bumps and two half bumps for all three Prandtl numbers. The mushy zone shows a wavy shape. There are six vortices known from the velocity vector distribution. The current stage is characterized by convective heat transfer, with natural-convection exerting the dominant influence, thereby resulting in a more pronounced distribution of temperature field and velocity vector. In addition, the heat transfer capacity and momentum diffusion capacity decrease with increasing Prandtl number, resulting in slower melting rate and lower vortex height of wax. The melting patterns of the wax layers at 45°, 0° and –45° positions are similar for the three Prandtl numbers. A large vortex exists in the melted liquid wax as shown by the velocity vector distribution. The liquid zone changed more significantly with melting than at the beginning of wax melting. The liquid zone presents the shape of a half funnel. This is attributed to the fact that the melting of wax is at the stage of convective development, and the heat transfer mode is dominated by a combination of conduction and convection. The heat from the lower part is continuously carried to the upper part by the buoyancy force and the melted liquid wax flushes the mushy zone, resulting in a faster melting of the wax in the upper part and a slower melting of the wax in the lower part. The melting rate of wax at all three angles gradually slows down with the increase of Prandtl number. The temperature field isotherms at the three Prandtl numbers are uniformly distributed and parallel to the heat transfer surface at –90°. The velocity of liquid wax is approximated as 0 by the velocity vector distribution. The heat source is oriented in the opposite direction the direction of buoyancy, resulting in a suppression of natural-convection at –90°. The sole mechanism for heat transfer is conduction. The temperature field and the ratio of liquid waxes at the three *Pr* numbers are less affected by the Prandtl number. The thermal diffusion effect caused by the variation in Prandtl number is not significant due to the limited melted liquid wax.

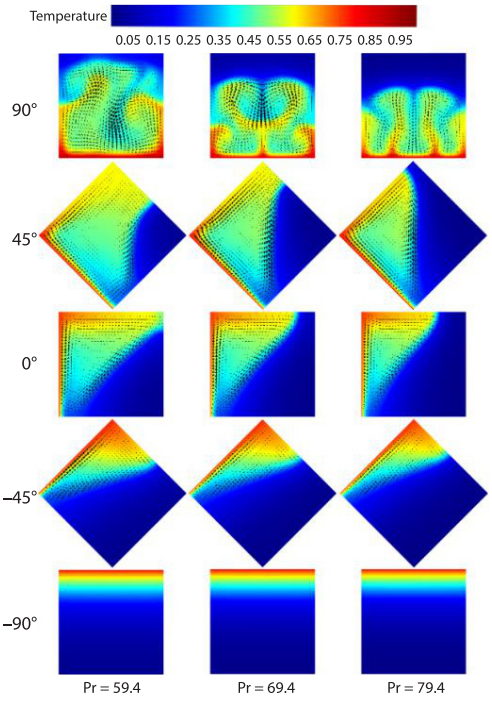

Figure 6. The temperature field (contour) and velocity vector distribution (arrow) of wax at different angles under different Prandtl numbers, (Fo = 0.052)

The liquid wax is gradually reduced and the melting pattern changes more significantly from 90° to –90° when Fo = 0.052 as shown in fig. 6. The temperature field appears to be violently disturbed and three large irregular vortices appear in the flow field at 90° when the Pr = 59.4. The velocity vector distribution has two large and four small vortices when Pr = 69.4. There are still six vortices in the velocity vector distribution when Pr = 79.4, and they are oblong and of similar size. Both the temperature and velocity vector distribution change significantly compared to the previous melting time point (Fo = 0.029) and the two vortices in the velocity vector distribution merge into one large vortex when Pr = 59.4. Both the temperature field pattern and the flow field change to the middle position at Pr = 69.4. Two vortices

are fusing positively into one large vortex as seen from the velocity vector distribution. The temperature and flow fields remain mainly in the vertical direction and the temperature field bulge and vortex height both grow higher at Pr = 79.4. The temperature and flow field patterns both change significantly at 90° as a result of the buoyancy force. The melting has entered the late stage, and convection is fully developed. The smaller the Prandtl number, the greater the melting rate. The primary mode of heat transfer occurs through convection at 45° and 0°. The proportion of liquid wax at both positions gradually decreases as the Prandtl number increases. The wax layer at both positions is in the later stages of melting when the Prandtl number is 59.4. Convection is partially inhibited at –45°. The mode of heat transfer is still dominated by a combination of conduction and convection at –45°. The rate of heat transfer is slower than the rate dominated by convection. The temperature field and velocity vector distributions at the three Prandtl numbers are similar in shape to those at the previous time point. The distribution of the temperature field and velocity vector remains largely unchanged compared to the previous time, and the influence of Prandtl is not significantly evident at –90°.

By comparing the changes of temperature field and velocity vector distribution of the wax layer at different Prandtl numbers, the results indicate that the change of Prandtl number has little influence on the initial melting of wax. This is due to the fact that the heat transfer at the beginning of the melting process is heat conduction and the melting process is short, resulting in less liquid wax being melted. Therefore, the change of heat transfer capacity caused by the change of Prandtl number is not obvious. The mode of heat transfer undergoes transformation, accompanied by alterations the shape and quantity of vortices, as the melting process advances. The melting rate of wax gradually increases as the Prandtl number decreases, which aligns with the findings reported in the literature [34]. Therefore, reducing the Prandtl number is helpful to improve the melting rate of wax during the wax removal process.

Effect of Prandtl number on wax velocity distribution at different angles

The impact of Prandtl number on the velocity distribution of the wax layer at different angles in the pipe-line when Fo = 0.052 is illustrated in fig. 7. The horizontal co-ordinate is the dimensionless length of the horizontal direction of the radial cross-section of the pipe-line. The vertical co-ordinate is the velocity variation of the wax in the direction perpendicular to the horizontal co-ordinate at 1/2 height of the selected micro-element square cavity ($Y/2$).

The velocity distribution at the 90° position of the wax layer is shown in fig. 7. The maximum rising velocity is 0.01619 and 0.01728 for Prandtl number values of 59.4 and 69.4, respectively, representing a significant increase of 97.92% and 111.25% compared to the Prandtl number value of 79.4. The melting process has reached the advanced stage with a Prandtl number value of 59.4, resulting in a slight decrease in speed. The velocity distribution at the 90° position is approximately symmetric about X/L = 0.5, with two maximum rising velocities of 0.01695 and 0.01728 at Pr = 69.4. The vortex approximation is symmetric about X/L = 0.5 combined with the velocity vector distribution in fig. 6. There are also two peaks of rising velocity and they are equal to 0.00818 when Pr = 79.4. The vortex is also symmetric about X/L = 0.5. The maximum sinking velocity increases 243.78% when Prandtl number decreases from 79.4 to 59.4. At the 45° position of the wax layer, the maximum rate of rise increases by 40.01% when the Prandtl number decreases from 79.4-59.4. The maximum sinking velocity appears to be different from the rising velocity pattern. The maximum sinking velocity increases when the Prandtl number decreases from 79.4 to 69.4 but shifts when it decreases to 59.4. The maximum sinking velocity at Pr = 59.4 is 0.00491 and occurs at 0.94. The upper part of the localized wax

layer at the selected location has melted when the Prandtl number is 59.4 as known from fig. 6. At the same time, it can be seen from the velocity vector distribution that the velocity vector distribution in the upper right half of the wax layer is relatively uniform, and this part is at *Y*/2, which is in a stable convective cycle state. Therefore, the sinking velocity of liquid wax changes little when the Pr = 59.4. The smaller the Prandtl number, the convective heat transfer capacity is enhanced, and both the maximum rising velocity and the maximum sinking velocity gradually increase at 0° and –45°. The maximum rising velocity increases by 38.14% and 15.98%, and the maximum sinking velocity increases by 16.02% and 3.86%, respectively, when Prandtl number decreases from 79.4-59.4. The wax at *Y*/2 does not melt at –90° due to the slow heat conduction, resulting in zero velocity change.

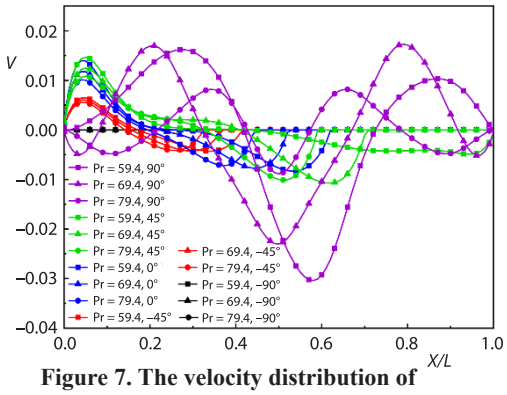

Figure 7. The velocity distribution of wax at different angles under different Prandtl numbers

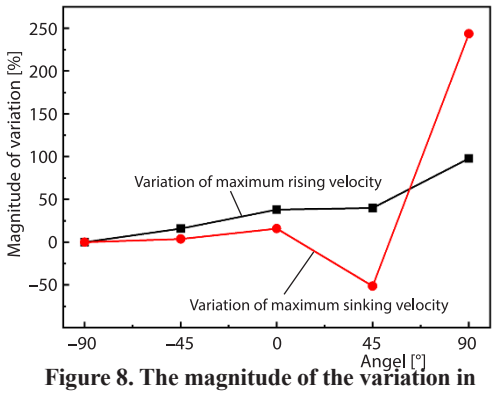

Figure 8. The magnitude of the variation in maximum rising and sinking velocity when the Prandtl number decreases from 79.4-59.4

In summary, decreasing the Prandtl number can effectively improve the convection velocity. In addition, it is found that the change of Prandtl number has different effects on the maximum rising and sinking velocities of wax layers at different positions. Combined with fig. 8, it can be intuitively found that the decrease of Prandtl number has an increasing trend on the maximum rising velocity of liquid wax from –90° to 90°. The maximum rising velocity increases at 90°, reaching 97.92%. The decrease of Prandtl number also shows an upward trend in the maximum sinking velocity of the wax layer from –90° to 90°. The inflection point at the 45° position is due to the fact that a stable convective circulation phase has been entered and the velocity has decreased when Pr = 59.4. The maximum sinking velocity still appears at 90°, and the velocity increases by 243.78%.

It is concluded that the influence of the decrease of Prandtl number on the maximum rising and sinking velocity of the wax layer from –90° to 90° is gradually enhanced. This is attributed to the fact that the angle between the direction of the buoyancy force and heat source gradually decreases, and the natural-convection is gradually enhanced from –90° to 90°. The increase of melted liquid wax leads to a more significant heat transfer capacity. The effect of Prandtl number on the maximum sinking velocity is greater than that on the maximum rising velocity at 90°, but the effect is reversed at –45°, 0°, and 45°. The change in velocity at –90° is not affected by the Prandtl number. The effect of natural-convection is greatest at 90°. The lower part of the local position has melted wax and convection is more adequate in combination with fig. 6. The unmelted wax in the upper part creates an obstacle to the uplift of the liquid wax. The situation is the opposite of the 90° position at –45°, 0° and 45°. The upper part of the local position is liquid wax, which can obtain sufficient convection heat transfer. Below is

unmelted paraffin, which impedes the downward flow. The –90° position is due to suppressed convection and no velocity change of wax.

Effect of Prandtl number on the area of three zones of wax at different angles

The wax layer is mainly composed of wax. For the multi-component mixture of wax, the melting point is a specific temperature range, and there are liquid zone, mushy zone and solid zone in the melting process. The thickness of the mushy zone influences the heat transfer and has an essential influence on the whole melting process of the wax layer. Therefore, analyzing the variation in the area of the three zones helps to dissect the effect of Prandtl number on the melting of the wax layer.

The variation of Prandtl number on the liquid fraction of the wax layer at different angles is shown in fig. 9. The variation of liquid fraction can directly indicate the influence of Prandtl number on the melting rate of wax. The melting rate of the wax layer at all angles is significantly increased with decreasing Prandtl number. This is due to the decrease in Prandtl number, which enhances the convective heat transfer and increases the melting rate of wax.

The time corresponds to the complete melting time of wax when the liquid fraction is 1. The complete melting time of the wax layer gradually decreases, exhibiting a non-linear change from –90° to 90° as depicted in fig. 10. The complete melting time of the wax layer is reduced by 23.78% when the Prandtl number is reduced from 79.4 to 59.4. The degree of influence on the complete melting time from –90° to 90° is gradually enhanced, which is shortened by 23.78 %, 24.52 %, 25.84 %, 26.58 %, and 29.80 %, respectively. Distinct differences in convection intensity due to the size of the angle between the direction of the buoyancy force and the direction of the heat source cause significant differences in the time to complete melting. By fitting the five angles that have been simulated under three Prandtl numbers, the relationship of eq. (20) is obtained. To provide a reference for estimating the duration of wax removal required during the thermal washing process.

$$\begin{aligned}
&\mathrm{Pr}=59.4:\mathrm{Fo}=-1.22\cdot10^{-7}\alpha^3+1.95\cdot10^{-5}\alpha^2-1.20\cdot10^{-3}\alpha+0.09\ (-90°\le\alpha\le90°)\\
&\mathrm{Pr}=69.4:\mathrm{Fo}=-1.24\cdot10^{-7}\alpha^3+2.19\cdot10^{-5}\alpha^2-1.44\cdot10^{-3}\alpha+0.11\ (-90°\le\alpha\le90°)\\
&\mathrm{Pr}=79.4:\mathrm{Fo}=-1.48\cdot10^{-7}\alpha^3+2.54\cdot10^{-5}\alpha^2-1.65\cdot10^{-3}\alpha+0.13\ (-90°\le\alpha\le90°)
\end{aligned}\tag{20}$$

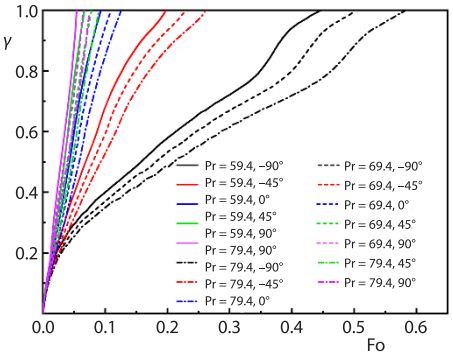

Figure 9. The variation of the liquid fraction of the wax at different angles under different Prandtl numbers

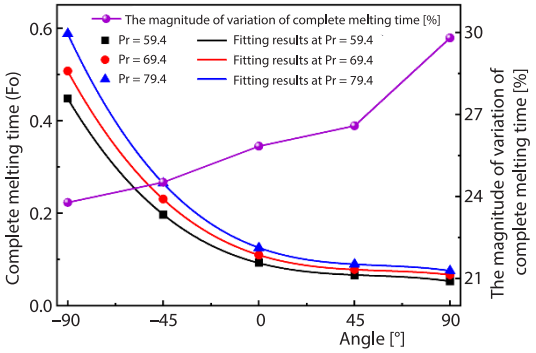

Figure 10. The complete melting time of wax at different angles with different Prandtl numbers and the magnitude of the variation of the complete melting time when the Prandtl number decreases from 79.4-59.4

From figs. 11 and 12, it can be found that the Prandtl number has a weak effect on the variation of the area of the mushy zone and the solid zone under the heat transfer mode dominated by conduction heat in the early stage. The percentage of mushy and solid zones changes more significantly as melting proceeds. The evolving relationship between the mushy zone and the Fourier number is obviously different from that between the liquid zone and solid zone and the Fourier number. The proportion of mushy areas at each angle of the wax layer shows a trend of increasing to a certain peak and then decreasing. The proportion of mushy zones fluctuates until it reaches a peak because the natural convective effect is the greatest and the convective intensity is higher at 90°. Other positions have less convection effect and more stable growth. The peak in the proportion of the mushy zone can be attributed to the fact that during the initial melting stage, the wax primarily undergoes heat conduction for transfer. As a result, there is a rapid increase in the overall temperature of the wax layer, leading to an accelerated rise in both liquid phase and mushy zone proportions. Convection is gradually involved in heat transfer as melting proceeds. The liquid wax flushes the mushy zone and accelerates the melting of the mushy zone. The proportion of the mushy zone reaches its maximum and subsequently decreases when the growth rate of the mushy zone equals the melting rate. Prandtl number has no effect on the peak of the mushy zone area at each angle is found by fig. 11. This is because the decrease in the Prandtl number only increases the melting rate and has no impact on the amount of heat required to melt the wax layer. The time required for the disappearance of the solid-phase zone is shorter with decreasing Prandtl number is shown in fig. 12. It is related to the fact that the decrease of Prandtl number indicates the enhancement of heat transfer energy, then the faster the heat transfer rate to the solid zone.

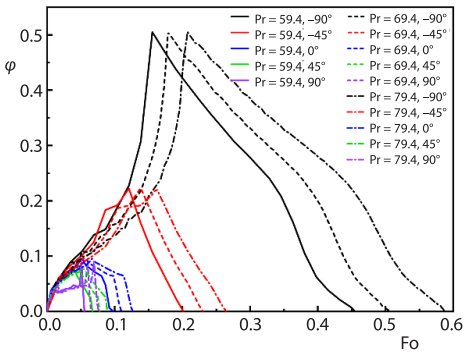

Figure 11. The variation of the mushy phase area ratio of the wax at different angles for various Prandtl numbers

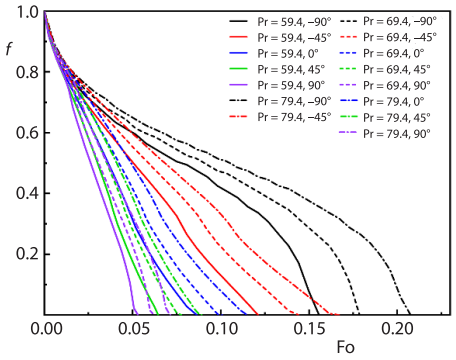

Figure 12. The variation of the solid phase area ratio of the wax at different angles for various Prandtl numbers

By analyzing the variation in the area of the three zones at each position of the wax layer, it is revealed that a smaller Prandtl number corresponds to a shorter time required for the complete melting of the wax layer. Meanwhile, it speeds up the transformation of the wax layer in the solid zone into a loose and porous mushy zone, which is more conducive to wax removal. In this study, the best Prandtl number is 59.4. The maximum rate of melting of wax when Prandtl number is 59.4. The rate of wax removal during the thermal wax removal process can be increased by reducing the Prandtl number of wax.

Conclusions

In this paper, the heat transfer process of phase change of the wax layer in the pipeline at different angles was simulated numerically based on the lattice Boltzmann method. The

heat transfer between the wax layer and the hot water is considered the convective heat transfer boundary. The effect of Prandtl number on the heat transfer law of phase change at local positions (90°, 45°, 0°, –45°, and –90°) of the wax layer was analyzed by the changes of temperature field, velocity vector distribution, flow velocity and area of three zones during the melting of the wax. The main conclusions are summarized as follows.

The flow velocity of the wax layer is influenced differently by the Prandtl number at various angles. The effect on the velocity was least at –90°, where the maximum rise and sink velocities were 0. The 90° position had the greatest effect on the velocity, increasing it by 97.92% and 243.78%, respectively. The decrease of Prandtl number can enhance the convection intensity and effectively increase the maximum rising and sinking rate of liquid wax and promote heat transfer.

The complete melting time of wax can be effectively reduced by decreasing the Prandtl number. The complete melting time of the wax layer is reduced by 23.78% and the effect of Prandtl number on the complete melting time of the wax layer at each angle is gradually increased from –90° to 90° when the Prandtl number decreases from 79.4-59.4. The melting time of the wax layer at each angle exhibits a non-linear relationship. An equation for the relationship between the angle of the wax layer and the complete melting time is fitted to give a reference for the actual thermal wax removal.

According to the principles of phase change heat transfer of the wax layer in the process of thermal washing, a synergistic method of thermal washing wax removal and chemical wax removal can be considered. Chemical agents are added to reduce viscosity and improve the wax removal rate in the process of thermal washing. The time required for the solid zone to transform into a mushy zone is less than the complete melting time and the wax layer melts the slowest at –90°. It can be considered to gradually reduce the temperature of hot water and control the flow rate of thermal washing to ensure that the bottom of the wax layer is covered, so as to reduce the energy loss in the later stage.

Acknowledgment

This work is supported by the National Natural Science Foundation of China (52076036 and the Natural Science Foundation of Heilongjiang Province of China (LH2020E017).

Nomenclature

c_p – specific heat capacity, [Jkg^{-1}K^{-1}]
$\mathbf{e}_i$ – lattice discrete velocity
En – enthalpy
$\mathbf{F}$ – total body force
Fo – Fourier number
F_ε – shape factor
f – distribution function for flow field
g – acceleration due to Earth's gravity
g_i – distribution function for temperature field
K – porous medium permeability
k_e – effective thermal conductivity, [Wm^{-1}K^{-1}]
La – latent heat [Jkg^{-1}]
L – local model length, [m]
Pr – Prandtl number
Ra – Rayleigh number
t_w – outermost temperature of the wax layer, [K]
Ste – Stefan number
T – temperature, [K]
t_f – hot water temperature, [K]
X, Y – dimensionless co-ordinates

Greek symbols

α – thermal diffusivity, [m^{2}s^{-1}]
β – thermal expansion coefficient
ε – porosity
γ – liquid fraction
ρ – density
ν – kinematic viscosity [m^{2}s^{-1}]
φ – mushy phase area of the wax

Subscripts

fl – liquid
fs – solid
ref – reference

References

[1] Yang, F., *et al*., Investigation on the Mechanism of Wax Deposition Inhibition Induced by Asphaltenes and wax Inhibitors, *Journal of Petroleum Science and Engineering*, *204* (2021), 108723
[2] Liu, X., *et al*., Numerical Simulation of Paraffin Melting in Circular Tube Using Lattice Boltzmann Method, *Thermal Science*, *26* (2022), 3A, pp. 2113-2123
[3] De Souza Mendes, P. R., *et al*., Startup Flow of Gelled Crudes in Pipe-Lines, *Journal of Non-Newtonian Fluid Mechanics*, *179-180* (2012), July, pp. 23-31
[4] Rehan, M., *et al*., Determination of Wax Content in Crude-Oil, *Petroleum Science and Technology*, *34* (2016), 9, pp. 799-804
[5] Boucetta, R., *et al*., Numerical Investigation of Wax Deposition Features in A Pipe-Line under Laminar Flow Conditions, *Journal of Petroleum Science and Engineering*, *217* (2022), 110929
[6] Fadairo, A., *et al*., Modelling of Wax Deposition during Oil Production Using a Two-Phase Flash Calculation, *Petroleum and Coal*, *52* (2010), 3, pp. 193-202
[7] Jiang, H., *et al.*, Numerical Study for Removing Wax Deposition by Thermal Washing for the Waxy Crude-Oil Gathering Pipe-Line, *Science Progress*, *103* (2020), 3, 36850420958529
[8] Gao, X., *et al*., Experimental Study on the Wax Removal Physics of Foam Pig in Crude-Oil Pipe-Line Pigging, *Journal of Petroleum Science and Engineering*, *205* (2021), 108881
[9] Wang, W., *et al*., Experimental Study on Wax Removal and Viscosity Reduction of Waxy Crude-Oil by Ochrobactrum Intermedium, *Journal of Petroleum Science and Engineering*, *213* (2022), 110445
[10] Zhang, H., *et al.*, Application of Superparamagnetic Nanoparticle (SPM-NP) Heating in Wax Removal during Crude-oil Pipe-line Pigging, *Energies*, *15* (2022), 17, 6464
[11] Ilyushin, P., *et al.*, Study of the Influence of Dosing Conditions of Wax Inhibitors on Its Efficiency Using Numerical Simulation, Proceedings of the Institution of Mechanical Engineers – Part E: *Journal of Process Mechanical Engineering*, (2023), On-line first, https://doi.org/10.1177/09544089231158191, 2023
[12] Liu, X., *et al.*, Phase Heat Transfer Characteristics and Influential Factors of Wax Removal by Hot Water in Pipe-Lines, *Chinese Science Bulletin*, *63* (2018), 11, pp. 1062-1070
[13] Li, X., *et al*., Numerical Investigation on the Melting Characteristics of Wax for the Safe and Energy-Efficiency Transportation of Crude-Oil Pipe-Lines, *Measurement: Sensors*, *10-12* (2020), 100022
[14] Zhou, Z., *et al.*, Numerical Study on Nusselt number of Moving Phase Interface during Wax Melting in Tube Using Lattice Boltzmann Method, *Thermal Science*, *26* (2022), 6B, pp. 4957-4967
[15] Ning, C., *et al*., Modelling Reacting Multi-Species Flows with a Detailed Multi-Fluid Lattice Boltzmann Scheme, *Thermal Science*, *25* (2021), 1B, pp. 691-704
[16] Qi, H., *et al*., Lattice Boltzmann simulation of Resistance Coefficient of the Oil and Water Migration in Porous Media, *Thermal Science*, *22* (2018), Suppl. 2, pp. S547-S556
[17] Asadi Abchouyeh, M., *et al*., Heat Transfer Enhancement Inside Channel by Using the Lattice Boltzmann Method, *Thermal Science*, *25* (2021), 5A, pp. 3543-3555
[18] Liu, X., *et al*., Numerical Study on the Effect of Thermal Diffusivity Ratio in Phase Change Heat Transfer of Crude-Oil Using Lattice Boltzmann Method, *Thermal Science*, *27* (2023), 2B, pp. 1627-1639
[19] Ganaoui, E., Alami E., A lattice Boltzmann Coupled to Finite Volumes Method for Solving Phase Change Problems, *Thermal Science*, *13* (2009), 2, pp. 205-216
[20] Lin, Q., *et al*., Lattice Boltzmann Simulation of Flow and Heat Transfer Evolution Inside Encapsulated Phase Change Materials Due to Natural-Convection Melting, *Chemical Engineering Science*, *189* (2018), Nov., pp. 154-164
[21] Jourabian, M., *et al*., Lattice Boltzmann Simulation of Melting Phenomenon with Natural-Convection from an Eccentric Annulus, *Thermal Science*, *17* (2013), 3, pp. 877-890
[22] Cailei, L., *et al*., Effect of Heating Modes On Melting Performance of a Solid-Liquid Phase Change Using Lattice Boltzmann Model, *International Communications in Heat and Mass Transfer*, *108* (2019), 104330
[23] Zhao, Y., *et al*., Comparative Study of Natural-Convection Melting Inside a Cubic Cavity Using an Improved Two-Relaxation-Time Lattice Boltzmann Model, *International Journal of Heat and Mass Transfer*, *143* (2019), 118449
[24] Dai, R., *et al.*, Evolution of Natural-Convection Melting Inside Cavity Heated from Different Sides Using Enthalpy Based Lattice Boltzmann method, *International Journal of Heat and Mass Transfer*, *121* (2018), June, pp. 715-725
[25] Rao, Z., *et al.*, The Lattice Boltzmann Investigation for the Melting Process of Phase Change Material in an Inclined Cavity, *Journal of Heat Transfer*, *140* (2018), 1, 012301

[26] Voller, V. R., *et al.*, A Fixed Grid Numerical Modelling Methodology For Convection-Diffusion Mushy Region Phase-Change Problems, *International Journal of Heat and Mass Transfer*, *30* (1987), 8, pp. 1709-1719
[27] Su, Y., Davidson, J. H., A New Mesoscopic Scale Timestep Adjustable Non-Dimensional Lattice Boltzmann Method for Melting and Solidification Heat Transfer, *International Journal of Heat and Mass Transfer*, *92* (2016), Jan., pp. 1106-1119
[28] Guo, Z., Zhao T. S., A Lattice Boltzmann Model for Convection Heat Transfer in Porous Media, Numerical Heat Transfer – Part B: *Fundamentals*, *47* (2005), 2, pp. 157-177
[29] Seta, T., *et al*., Lattice Boltzmann Simulation of Natural-Convection in Porous Media, *Mathematics and Computers in Simulation*, *72* (2006), 2-6, pp. 195-200
[30] Gao, D., Chen, Z., Lattice Boltzmann Simulation of Natural-Convection Dominated Melting in A Rectangular Cavity Filled With Porous Media, *International Journal of Thermal Sciences*, *50* (2011), 4, Sept., pp. 493-501
[31] Guo, Z., Zhao T. S., Lattice Boltzmann Model for Incompressible Flows through Porous Media, *Physical Review E*, *66* (2002), 3, 036304
[32] Shi, B., Guo, Z., Lattice Boltzmann Model for Non-Linear Convection-Diffusion Equations, *Physical Review E*, *79* (2009), 1, 016701
[33] Zhang, T., *et al*., General Bounce-Back Scheme for Concentration Boundary Condition in the Lattice-Boltzmann Method, *Physical Review E*, *85* (2012), 1, 016701
[34] Li, D., *et al*., Lattice Boltzmann Models for Axisymmetric Solid-Liquid Phase Change, *International Journal of Heat and Mass Transfer*, *112* (2017), Sept., pp. 795-804

Paper submitted: July 6, 2023
Paper revised: October 15, 2023
Paper accepted: October 23, 2023